Biochimie 115 (2015) 136–143

Contents lists available at ScienceDirect

Biochimie

journal homepage: www.elsevier.com/locate/biochi

Research paper

Expanding the chemical space of polyketides through structure-guided mutagenesis of *Vitis vinifera* stilbene synthase

Namita Bhan [a, 1], Brady F. Cress [a], Robert J. Linhardt [a, b, c, d], Mattheos Koffas [a, c, *]

[a] Department of Chemical and Biological Engineering, Rensselaer Polytechnic Institute, Center for Biotechnology and Interdisciplinary Studies, Troy, NY, USA
[b] Department of Chemistry and Chemical Biology, Rensselaer Polytechnic Institute, Center for Biotechnology and Interdisciplinary Studies, Troy, NY, USA
[c] Department of Biological Sciences, Rensselaer Polytechnic Institute, Center for Biotechnology and Interdisciplinary Studies, Troy, NY, USA
[d] Department of Biomedical Engineering, Rensselaer Polytechnic Institute, Center for Biotechnology and Interdisciplinary Studies, Troy, NY, USA

ARTICLE INFO

Article history:
Received 9 April 2015
Accepted 22 May 2015
Available online 3 June 2015

Keywords:
Stilbene synthase
Aromatic polyketides
Type III polyketide synthases
Flavonoids
Resveratrol

ABSTRACT

Several natural polyketides (PKs) have been associated with important pharmaceutical properties. Type III polyketide synthases (PKS) that generate aromatic PK polyketides have been studied extensively for their substrate promiscuity and product diversity. Stilbene synthase-like (STS) enzymes are unique in the type III PKS class as they possess a hydrogen bonding network, furnishing them with thioesterase-like properties, resulting in aldol condensation of the polyketide intermediates formed. Chalcone synthases (CHS) in contrast, lack this hydrogen-bonding network, resulting primarily in the Claisen condensation of the polyketide intermediates formed. We have attempted to expand the chemical space of this interesting class of compounds generated by creating structure-guided mutants of *Vitis vinifera* STS. Further, we have utilized a previously established workflow to quickly compare the wild-type reaction products to those generated by the mutants and identify novel PKs formed by using XCMS analysis of LC-MS and LC-MS/MS data. Based on this approach, we were able to generate 15 previously unreported PK molecules by exploring the substrate promiscuity of the wild-type enzyme and all mutants using unnatural substrates. These structures were specific to STSs and cannot be formed by their closely related CHS-like counterparts.

1. Introduction

Polyketides (PKs) are a chemically important class of compounds with several beneficial pharmaceutical properties [1,2]. Natural PKs generated by type III polyketide synthases (PKSs) have been associated with the slowing of the aging process in model organisms [3,4], anti-inflammatory and anti-cancer properties [5–10] and have shown potential to ameliorate diabetes and nervous system disorders related complications [11,12]. Type III PKSs are found in several plants, bacteria and fungi [13–15]. They are homodimeric enzymes that catalyze iterative condensation of repeating units to a CoA-tethered starter substrate through a conserved Cys-His-Asn catalytic triad. Functionally diverse type III PKSs arise due to variable substitutions in non-catalytic residues present in the three catalytically important cavities: the substrate binding pocket, composed of the important residues S133, Q192, T194, T197, S338; the CoA binding tunnel, composed of L55, R58, L62; and the cyclization pocket, composed of T132, M137, F215, I254, G256, F265, P375 (residues numbered according to the *Vitis vinifera* stilbene synthase (*Vv*STS)). Altering these residues results in diversity of preference for starter substrates, number of extender substrates incorporated through iterative condensations and mechanism of cyclization of the poly-β-keto intermediate formed through Claisen condensation, aldol condensation or lactonization. Moreover, type III PKSs possess unusually broad substrate promiscuity and can accept several non-natural substrates to form novel non-natural PKs [2,16]. Apart from the naturally occurring type III PKSs, several intuitive and structure-guided mutations have also been carried out to alter their enzymatic activity, so as to expand the chemical diversity of PKs [17,18]. Some of the novel non-natural PKs formed through these processes has also been demonstrated to possess important biological activities [16].

Abbreviations: PKS, polyketide synthase; PK, polyketide; *Vv*, *Vitis vinifera*; STS, stilbene synthase; CHS, chalcone synthase; Wt, wild-type; HBN, hydrogen-bonding network; BNY, bisnoryangonin; CATL, *p*-coumaroyltriacetic acid lactone.

* Corresponding author.
E-mail address: koffam@rpi.edu (M. Koffas).
[1] Present address: Northwestern University, Evanston, Illinois, USA.

http://dx.doi.org/10.1016/j.biochi.2015.05.019
0300-9084/

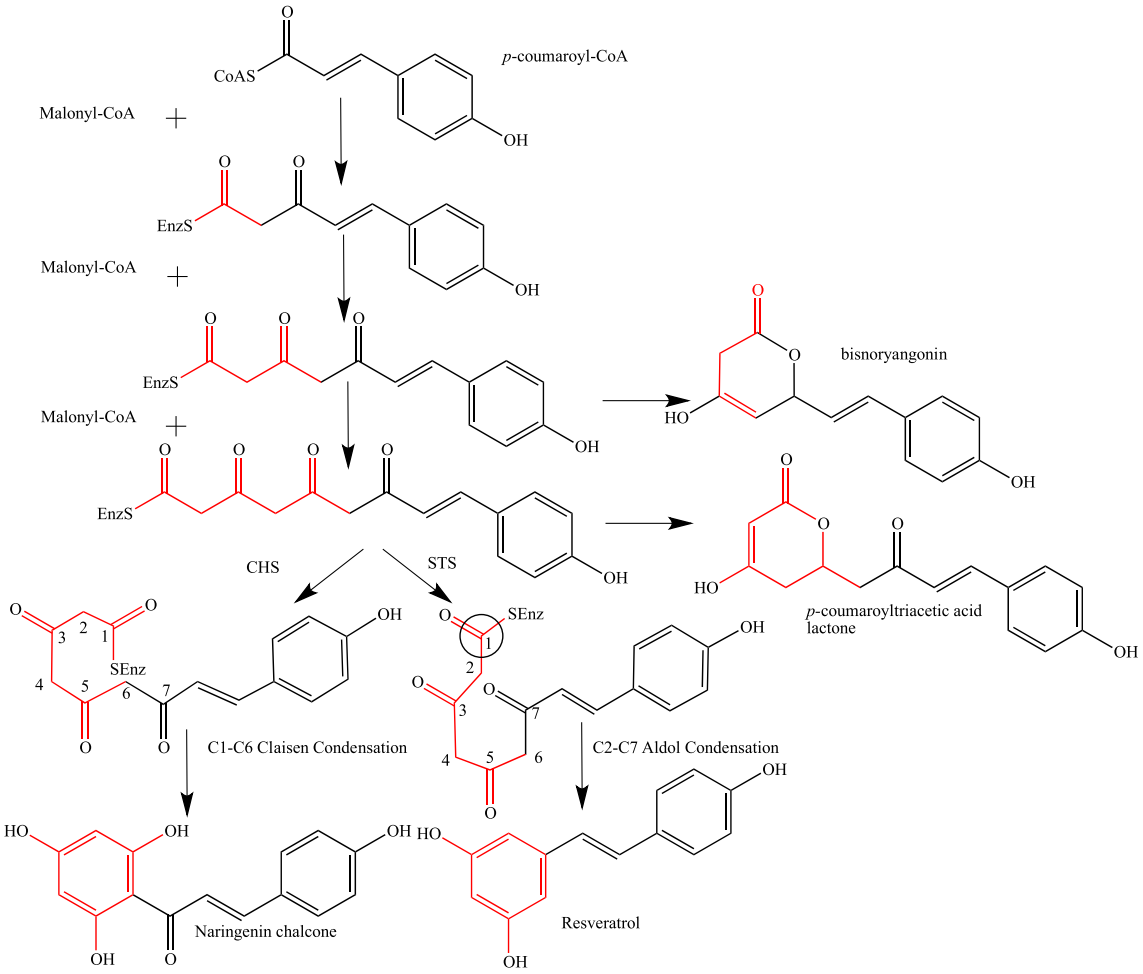

Fig. 1. General reaction catalyzed by wild type STS and CHS. STS and CHS react with their natural substrates, *p*-coumaroyl-CoA and malonyl-CoA to form primarily resveratrol and naringenin chalcone respectively. Bisnoryangonin (BYN) and *p*-coumaroyltriaceticacid lactone are natural derailment products of the reaction.

Stilbene synthase (STS) belongs to the type III PKS super family and is unique due to the presence of a hydrogen-bonding networks (HBN) [19], which is absent in the closely related chalcone synthase-like (CHS) enzymes (70–90% sequence similarity to STS). Due to the presence of this HBN, STS-like type III PKSs cyclize their polyketide intermediate through an aldol condensation reaction. CHS-like type III PKSs, in contrast, cyclize their intermediate primarily through a Claisen condensation (Fig. 1). While both STS and CHS form a tetraketide intermediate with *p*-coumaroyl-CoA and three molecules of malonyl-CoA, STS cyclizes the intermediate into resveratrol through a C2–C7 aldol condensation in contrast to CHS, which cyclizes the intermediate into naringenin chalcone through a C1–C6 Claisen condensation. Both enzymes form bisnoryangonin (BNY) and *p*-coumaroyltriacetic lactone (CTAL) as derailment products during the reaction [20].

We attempted to exploit the novel thioesterase-like property of STSs to further diversify the chemical space of PKs. Along these lines we created 6 mutants of *Vitis vinifera* stilbene synthase (*Vv*STS) and challenged these with non-natural substrates (Table 1).

2. Materials and methods

2.1. Site-directed mutagenesis

The plasmids expressing the his-tagged *Vv*STS and *Vv*STS T197G mutant were obtained from our previous studies [21].

Table 1
Table summerizing the results obtained in this study. List of PKs formed by the mutants created in this study. Cavity 1 is size of the cycliztion pocket calculated from CASTp. Cavity 2 is the size of the substrate binding pocket calculated from CASTp. The novel previously unreported PKs are highlighed in bold. "–" denotes reactions not tested.

Enzyme	Cavity 1 (Å^3)	Cavity 2 (Å^3)	Propionyl-CoA	Myristoyl-CoA	Octanoyl-CoA	Methylmalonyl-CoA
Wt	721.4	265.2	**1,2,3**	**4**	5	**6,7**
L214I	705.7	291.4	**1.2.3**	–	–	–
T197A	743.1	293	**2,8,9**	**10,11**	5,**12**	**6,13**
T197G	1134.3[a]		**1,14**	**4**	**15,16**	**6,7**
T197IG256L	612.4	265.2	**1,2,8,9**	–	–	**6,7**
T197M	635	265.2	–	–	–	**7**
T197GG265L	1016.6[a]		–	–	5,**12,16**	–

[a] The T197G and the T197GG256L mutations result in merging of the two cavities, we thus mention the size of the entire cavity in these cases.

The rest of the *Vv*STS mutants were constructed for this study with a QuickChange Site-Directed Mutagenesis Kit (Stratagene) according to the manufacturer's protocol and using the primers in Supplementary Table S1. Each construct was sequence analyzed to confirm the point mutation. The double mutants were created sequentially.

2.2. Protein expression and purification

After confirmation of the sequence, the plasmid was transformed *into Escherichia coli* BL21* (DE3). The cells harboring the plasmid were cultured to an OD_{600} of 0.6 in LB medium containing chloramphinecol (30 μg/ml) at 37 °C. Subsequently, isopropylthio-β-D-galactopyranoside (IPTG) (1.0 mM) was added to induce protein expression, and the cells were further cultured at 30 °C for 4 h. All of the following procedures were performed at 4 °C. *E. coli* cells were harvested by centrifugation at 4000 × g and frozen at −80 °C until further processing. The cells were disrupted by incubating with lysis buffer (50 mM NaH_2PO_4, 300 mM NaCl, 10 mM imidazole, pH 8.0), lysozyme (10 mg/ml) and 1 culture volume of Benzonase® nuclease (3 units/ml) at 4 °C for 30 min. The lysate was then centrifuged at 12,000 × g for 30 min. The supernatant was loaded onto a Ni-NTA spin column (Qiagen) pre-equilibrated with lysis buffer. The column was then washed with wash buffer (50 mM NaH_2PO_4, 300 mM NaCl, 20 mM imidazole, pH 8.0). The protein was eluted from the column using elution buffer (50 mM NaH_2PO_4, 300 mM NaCl, 300 mM imidazole, pH 8.0). The protein concentration was determined by the Bradford method (Protein Assay, Bio-Rad) with bovine serum albumin as the standard.

2.3. Enzymatic reaction

The reaction mixture contained starter substrate [4-coumaroyl-CoA (54 μM), octanoyl-CoA (54 μM), propionyl-CoA (54 μM), methylmalonyl-CoA (54 μM), or myristoyl-CoA (54 μM)], extender substrate [malonyl-CoA (108 μM) or $^{13}C_3$-malonyl-CoA (108 μM)], and the purified enzyme (20 μg) in potassium phosphate buffer (500 μl, 100 mM, pH 7.0). The purified enzyme was added to the reaction mixture last. Incubations were performed at 30 °C for 30 min and were stopped by the addition of ethyl acetate (500 μl) with 1% HCl. The extracted products (ethyl acetate extracts) were then concentrated in a speed vacuum and re-suspended in ethyl acetate (10 μl), and centrifuged at 14000 rpm for 10 min before running on a column. The products were separated by reverse-phase HPLC (Agilent 1260) on a Zorbax C18 column (4.6 × 150 mm, 5 μm, at a flow rate of 0.7 ml/min). Gradient elution was performed with H_2O and acetonitrile (ACN), both containing 0.2% trifluoroacetic acid: 0–7 min, 20% ACN; 7–15 min, linear gradient from 20% to 60% ACN; 15–30 min, linear gradient from 60% to 70% ACN; 30–36 min, linear gradient from 70% to 30% ACN. Three reactions (technical replicates) were pooled into ethyl acetate (10 μl) for LC-MS analysis. Online HR–ESI-LCMS spectra were measured with an Agilent Technologies HPLC 1200 series HPLC coupled to a Thermo Scientific LTQ Orbitrap XLTM mass spectrometer fitted with an electrospray ionization (ESI) source. The ESI capillary temperature and the capillary voltage were 320 °C and 4.0 V, respectively. The tube lens offset was set at 20.0 V. All spectra were obtained in the negative and positive mode, over a mass range of *m/z* 150–700, and at a range of one scan every 0.2 s. The collision gas was helium, and the relative collision energy scale was set at 30.0% (1.5 eV). Dependent MS/MS scans were acquired for the first four most abundant parent ions.

2.4. Substrates

4-Coumaroyl-CoA was chemically synthesized as previously described [22]. $^{13}C_3$-malonyl-CoA, malonyl-CoA, propionyl-CoA, octanoyl-CoA, methylmalonyl-CoA, myristoyl-CoA were purchased from Sigma.

2.5. XCMS workflow for analyzing online LCMS data

The workflow established included creating the structure-based mutants and carrying out the *in vitro* enzymatic reactions. The *in vitro* reactions were run with and without the $^{13}C_3$-malonyl-CoA for easier identification of novel PK structure from the HR-LC-MS/MS analysis. The reaction extracts were then run on the LC-MS to obtain online HR-LCMS (±5 ppm accuracy) which was finally compared using XCMS to directly calculate the fold change in production of PKs in the mutants compared to the wild-type and to identify peaks unique to the mutant. Raw data was converted to XML format using R processor (Script S1, obtained from http://www.metabolomics.strath.ac.uk/showPage.php?page=processingscripts), and analyzed using XCMS online [23]. XCMS was utilized for calculating fold changes in CTAL and BNY and all other peaks common to the wild type and mutant proteins (Fig. 6). All calculations were based on triplicates. This workflow obviated thin-layered chromatography (TLC) analysis of the reaction products and utilization of radioactive substrates for identification of products unique to the mutants.

2.6. Homology modeling and cavity size analysis

The models of the Wt *Vv*STS and the all the mutants were generated by the SWISS-MODEL package (http://expasy.ch/spdbv/) provided by the Swiss-PDB-Viewer program [24] based on the crystal structure of wild-type STS from *Acharis hypogaea* (PDB code: 1Z1E). The model quality was assessed using PROCHECK [25]. In the Ramachandran plot calculated for the model, most of the amino acid residues were present in the energetically allowed regions with only a few exceptions, primarily Gly residues that can adopt phi/psi angles in all four quadrants. The cavity volume was calculated by the program CASTP (http://cast.engr.uic.edu/cast/) [26].

3. Results

3.1. Substrate promiscuity of wild-type VvSTS

Several non-natural substrates have been supplied to wild-type *Acharis hypogea* STSs, resulting in the formation of mainly CATL and BYN-type pyrones [27,28]. We first investigated the substrate promiscuity of wild-type *Vv*STS (Wt *Vv*STS) with non-natural substrates that have not been tested previously. Specifically, we supplied Wt *Vv*STS with starter substrates of varying size: propionyl-CoA, myristoyl-CoA, octanoyl-CoA and methylmalonyl-CoA; malonyl-CoA was used primarily as the extender substrate for all of the reactions (Fig. 2).

Malonyl-CoA and methylmalonyl-CoA or propionyl-CoA acted as extender substrates in case of compounds **2, 3** & **7**, as is clearly indicated in the color-coding in Fig. 3. The Wt *Vv*STS accepted all of these aliphatic compounds as substrates to afford non-natural PKs (Fig. 3).

Propionyl-CoA and malonyl-CoA resulted in the formation of 3 major products. Compound **1** with the parent ion peak $[M + FA\text{-}H]^-$ at *m/z* 241.0700, a resorcinol derivative. Compound **2** with parent ion peak $[M-H]^-$ at *m/z* 263.1290 and **3** with *m/z* 323.1392, a

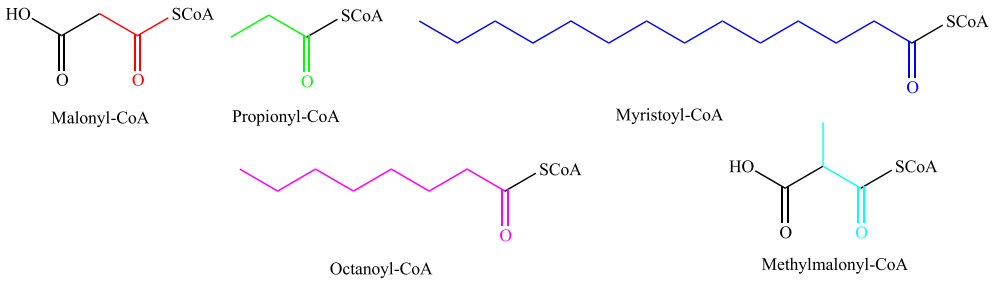

Fig. 2. Substrates utilized in this study. Color-coded substrates; for subsequent ease of understanding of PK structures generated by the wild-type and the mutants enzymes.

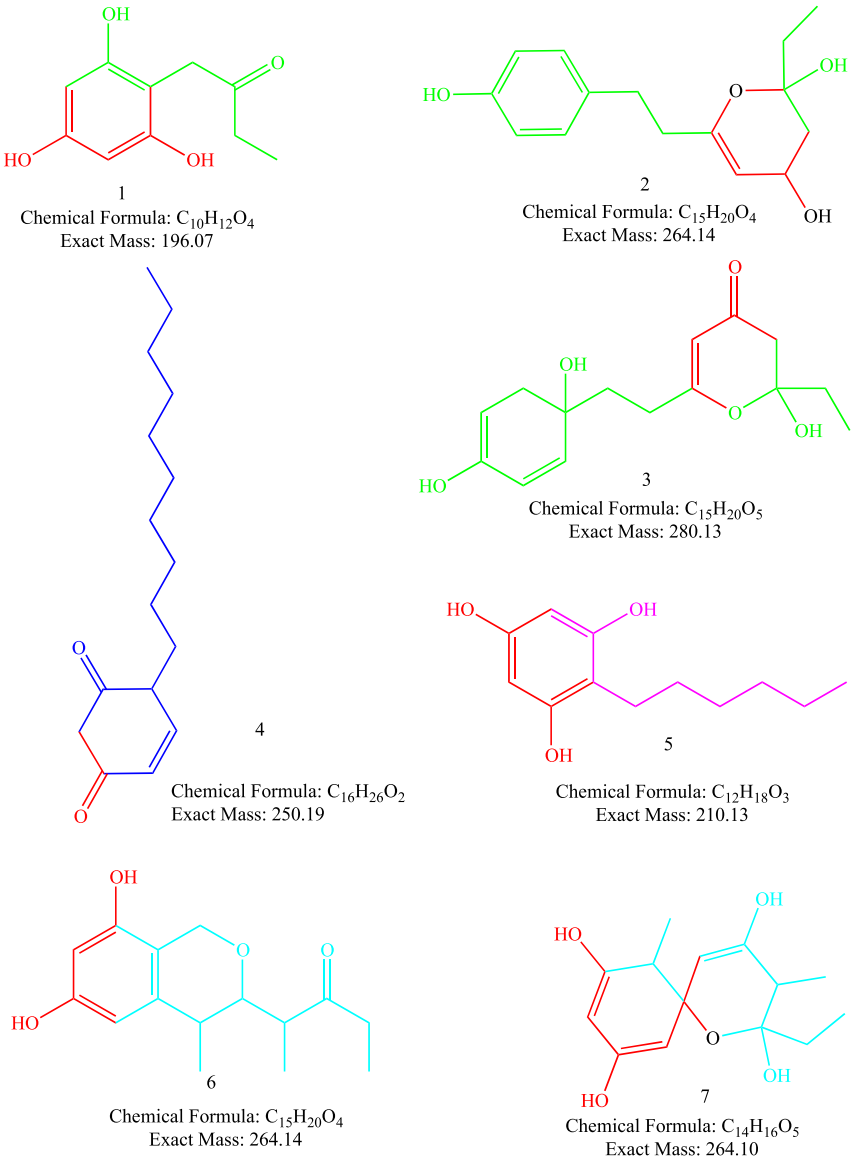

Fig. 3. Wt *Vv*STS accepts all the tested non-natural substrates to form PKs. Non-natural PKs formed by Wt *Vv*STS when supplied with non-natural substrates like propionyl-CoA (compounds **1**–**3**), myristoyl-CoA (compound **4**), octanoyl-CoA (compound **5**), or methylmalonyl-CoA (compounds **6** & **7**) as starter substrates, coupled with malonyl-CoA as the extender substrate.

$[M + COO^-]^-$ ion (Fig. 3, Supplementary Table S2 for MS details). Myristoyl-CoA and malonyl-CoA formed carboxylic acid **4**, which displayed a parent ion peak $[M + FA\text{-}H]^-$ at *m/z* 293.1756 (Fig. 3, Supplementary Table S2). Octanoyl-CoA and malonyl-CoA resulted in the formation of primarily a phlorophenone (**5**) with the parent ion $[M-H]^-$ at *m/z* 209.1185 (Fig. 3, Supplementary Table S2). Methylmalonyl-CoA and malonyl-CoA resulted in the formation of two non-natural PKs, a pentanone **6** at *m/z* 263.1274 $[M - H]^-$ and a pyranone **7** at *m/z* 307.1292 $[M + COO^-]^-$ (Fig. 3, Supplementary Table S2).

3.2. Substrate promiscuity of structure-based mutants of VvSTS

Next we tested the above substrates with the structure-based mutants of *Vv*STS. As hypothesized, perturbation of residues in the catalytically relevant pockets of *Vv*STS altered its substrate promiscuity. We supplied relevant substrates to each mutant based on predicted change in the properties of the catalytically relevant pockets; so all substrates were not supplied to all mutants. The mutants created led to the formation of novel, non-natural PKs that have not been reported previously (Figs. 4 and 5).

The leucine at position 214 is important for the structure of the cyclization pocket. Not surprisingly, replacing it with isoleucine (L214I) did not significantly alter the product profile. Compared to Wt VvSTS, mutant L214I led to a 14.4-fold, 27-fold, and 9.4-fold increase in production of compounds **1**, **2**, and **3**, respectively, when propionyl-CoA was used as a starter substrate (Fig. 3, Supplementary Fig. S1). This could be explained by the increase in the starter substrate binding pocket from 265.2 $Å^3$ for Wt *Vv*STS to 291.4 $Å^3$ in the L214I mutant, making it easier for the mutant to utilize propionyl-CoA as the substrate. The decrease in the cyclization pocket from 721.4 $Å^3$ to 705.7 $Å^3$ explains the absence of formation of any longer PKs.

Upon increasing the size of the cyclization pocket from 721.4 $Å^3$ to 743.1 $Å^3$ and the substrate-binding pocket from 265.2 $Å^3$ to 293 $Å^3$ by replacing the tyrosine at position 197 with an alanine, *Vv*STS T197A catalyzed formation of 5 new PKs unique to the mutant. Propionyl-CoA and malonyl-CoA resulted in the formation of two novel compounds, a benzoic acid with $[M-H]^-$ *m/z* of 279.0858 (**8**) and a phlorophenone with *m/z* 233.0811 $[M-2H]^-$ (**9**) (Fig. 4). In both **8** & **9** propionyl-CoA was utilized as an extender substrate as well. A 1.2-fold increase in the production of the **2**263.1290 with *m/z* 331.2014 $[M + CH_3COO^-]^-$ was observed (Supplementary Fig. S2). Upon supplying myristoyl-CoA and malonyl-CoA as the starter substrate and the extender substrate, respectively, two unique, novel phlorophenones were formed; **10** with a parent ion peak $[M-H]^-$ at 335.20, and **11** with a parent ion peak of $[M + FA-H]^-$ at 337.2016 (Fig. 4). Octanoyl-CoA and malonyl-CoA were also utilized by T197A to form **5** but 30-fold lower than the amount formed by the wild-type (Supplementary Fig. S2). Instead, the novel phlorophenone **12** with *m/z* $[M-H]^-$ of

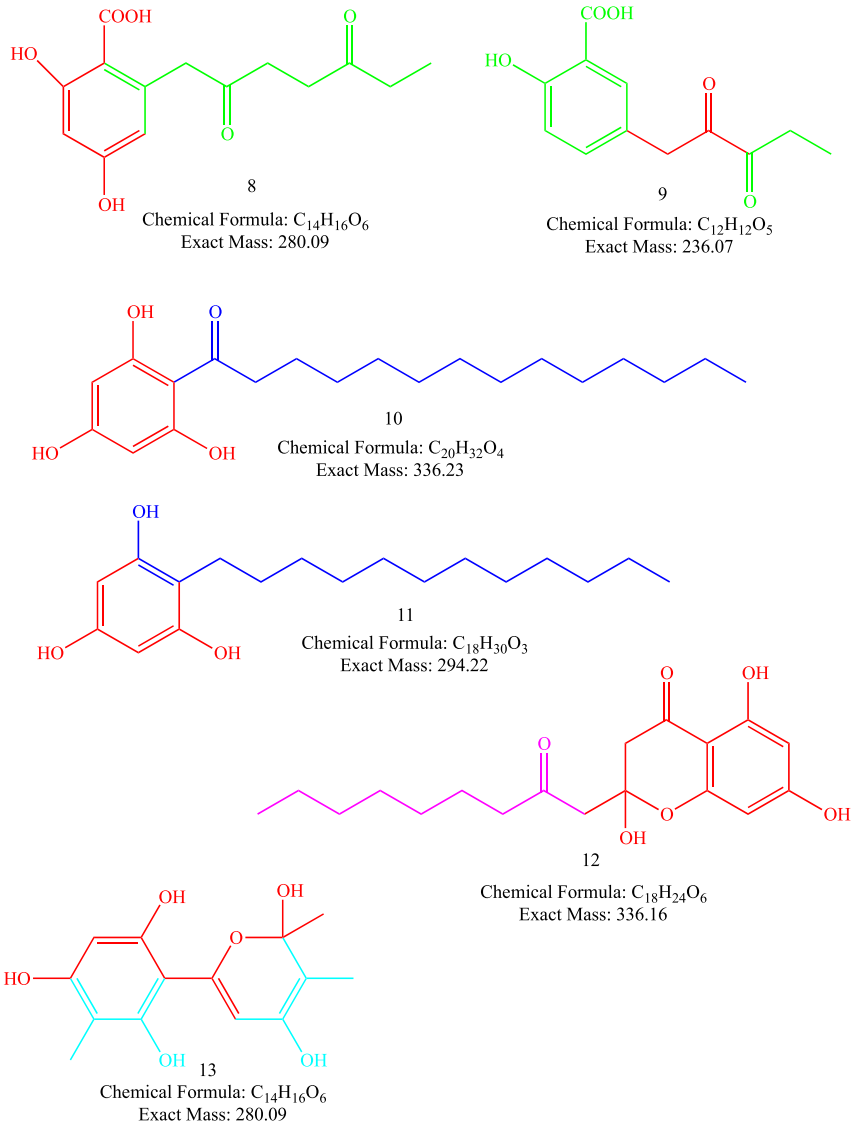

Fig. 4. Non-natural PKs (8–13) formed by mutant *Vv*STS. Novel PKs formed by the mutants when supplied with propionyl-CoA (compounds **8** and **9**), myristoyl-CoA (compounds **10** and **11**), octanoyl-CoA (compound **12**) and methylmalonyl-CoA (compound **13**) as starter substrates, coupled with malonyl-CoA primarily as the extender substrate.

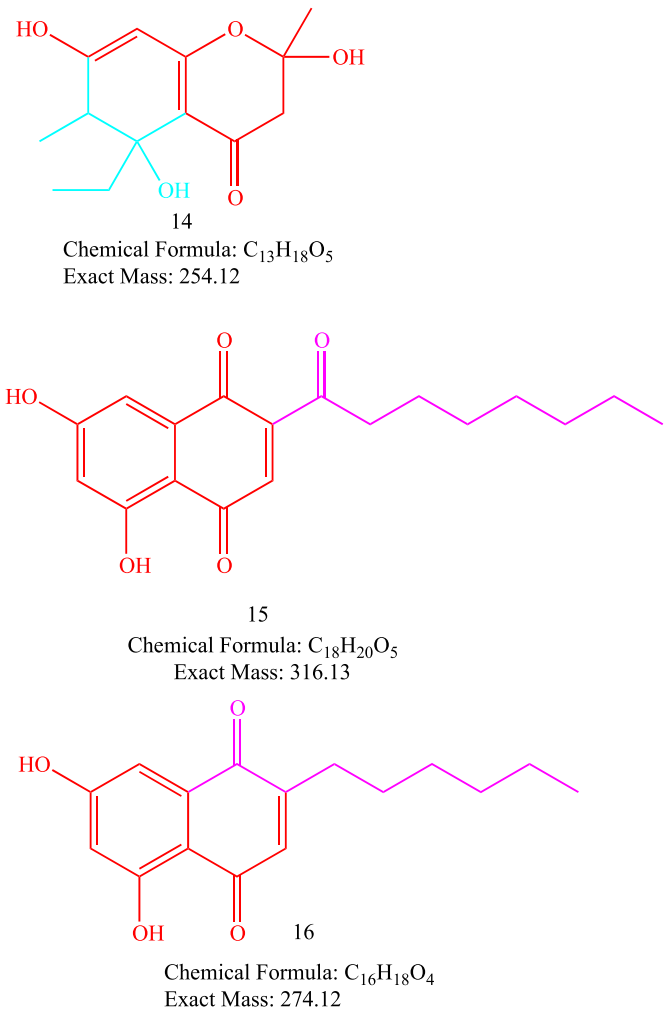

Fig. 5. Non-natural PKs (14–16) formed by mutant *Vv*STS. Novel PKs formed by the mutants created with methylmalonyl-CoA (compound **14**) and octanoyl-CoA (compounds **15** and **16**) as starter substrates, coupled with malonyl-CoA as extender substrate.

335.1488 was formed as the major product (Fig. 4). Methylmalonyl-CoA and malonyl-CoA as substrates resulted in the formation of the novel isochromanone **13** with the parent ion peak of $[M-H]^-$ 279.0858 (Fig. 4), where methylmalonyl-CoA was utilized as both extender and starter substrate. A 7.3-fold increase in the production of **6** was observed (Supplementary Fig. S2). The increase in size of both cyclization and substrate binding pocket of the mutant accommodated the formation of longer PKs.

Mutating the threonine at position 197 to glycine (T197G), as previously reported [21], results in the joining of the cyclization and substrate binding pockets, with a total cavity size of 1134.3 $Å^3$ as compared to 1029.2 $Å^3$ for Wt *Vv*STS. Propionyl-CoA and malonyl-CoA formed novel PK **14** (Fig. 5) with a parent ion $[M + Cl]^-$ *m/z* of 291.0994, again propionyl-CoA acted as both starter and extender substrate. A 4.1 fold decrease in formation of **1** was observed (Supplementary Fig. S3). Myristoyl-CoA and malonyl-CoA resulted in the formation of **4** with a 1.1-fold decrease as compared to Wt *Vv*STS (Supplementary Fig. S3). Octanoyl-CoA and malonyl-CoA resulted in the formation of two new PKs **15** and **16** with parent ion peaks $[M-H]^-$ of *m/z* 315.1261 and 273.1162 respectively (Fig. 5). Methylmalonyl-CoA and malonyl-CoA resulted in a 6.4-fold increase in formation of **7** and 7.1-fold increase in formation of **6** in comparison to the Wt *Vv*STS (Supplementary Fig. S3).

Next we created a double mutant, replacing the threonine at position 197 to an isoleucine and the glycine at position 256 to a leucine (T197IG256L). This resulted in a decrease of the cyclization pocket from 721.4 $Å^3$ to 612.4 $Å^3$ without significant change in the substrate binding pocket size. We did not carry out the *in vitro* reaction with myristoyl-CoA or octanoyl-CoA as we did not expect the mutant to form any novel PKs with these bulkier substrates. Propionyl-CoA and malonyl-CoA were utilized as substrates by T197IG256L to form **1** and **2** at 6-fold and 2-fold lower levels, respectively, than the wild-type (Supplementary Fig. S4). Moreover, compounds **8** and **9,** formed by T197A, were also formed by T197IG256L. The mutant did not form any new PKs with methylmalonyl-CoA and malonyl-CoA as substrates.

Replacing the threonine at position 197 with the bulkier methionine (T197M) resulted in a reduction of the substrate-binding pocket from 721.4 $Å^3$ to 635 $Å^3$. When we supplied methylmalonyl-CoA and malonyl-CoA as substrates, compound **7** was formed, however a 2.3-fold decrease in comparison to the Wt *Vv*STS was observed (Supplementary Fig. S4).

Upon creating the double mutant by replacing threonine at position 197 with a glycine and the glycine at position 256 with a leucine (T197GG256L), the homology model again predicted the merging of the cyclization and substrate binding pockets, except this time with a decreased volume of 1016.6 $Å^3$ as compared to 1029.2 $Å^3$ for Wt *Vv*STS. Surprisingly supplementation with propionyl-CoA and malonyl-CoA did not result in the formation of any significant products. Octanoyl-CoA and malonyl-CoA resulted in the formation of **12** and **5**, and **16**, however **15** was not formed in this case. Both **12** and **15** are formed from the same 18-carbon intermediate. Compound **12** is a derailment product, thus it is a pyrone, while formation of **15** requires cyclization by the enzyme. The absence of **15** can be explained by the possible incapability of the T197G256L mutant to successfully cyclize the longer PK intermediate (18 carbons). This is further supported by the significant increase in the amount of the derailment product **12** formed.

3.3. XCMS work-flow for analyzing the in vitro enzymatic reactions

We utilized a previously established workflow [21] for quick identification of non-natural PKs by the 6 mutants of *Vv*STS created in this study (Fig. 6). Briefly, enzymatic reactions were analyzed by high resolution LC-MS (HR-LCMS), and novel reaction products were automatically tabulated by comparison against the product profile of a control reaction using an online LC-MS data comparison analysis software known as XCMS [23,29]. Structural elucidation of novel reaction products was further aided by performing paired reactions, where one reaction used unlabeled malonyl-CoA and the other utilized stable-isotope labeled $^{13}C_3$-malonyl-CoA extender units. Novel parent ions were subjected to HR-LC-MS/MS, and comparison of fragmentation patterns between paired reactions enabled identification of novel products by tracking the additional mass conferred by incorporation of $^{13}C_3$-malonyl-CoA extender units.

4. Discussion

We have successfully diversified the PK space by creating structure-guided mutants of *Vv*STS, and supplying it with non-natural substrates. Specifically we altered the size of the substrate binding pocket (T197), the cyclization pocket (L214) and both (T197 & G256).

The data obtained demonstrated that wild-type *Vv*STS could utilize methylmalonyl-CoA, propionyl-CoA, octanoyl-CoA and myristoyl-CoA as starter substrates coupled with malonyl-CoA primarily as the extender substrate; of the 7 non-natural PKs generated by wild-type *Vv*STS, 6 have not previously been reported.

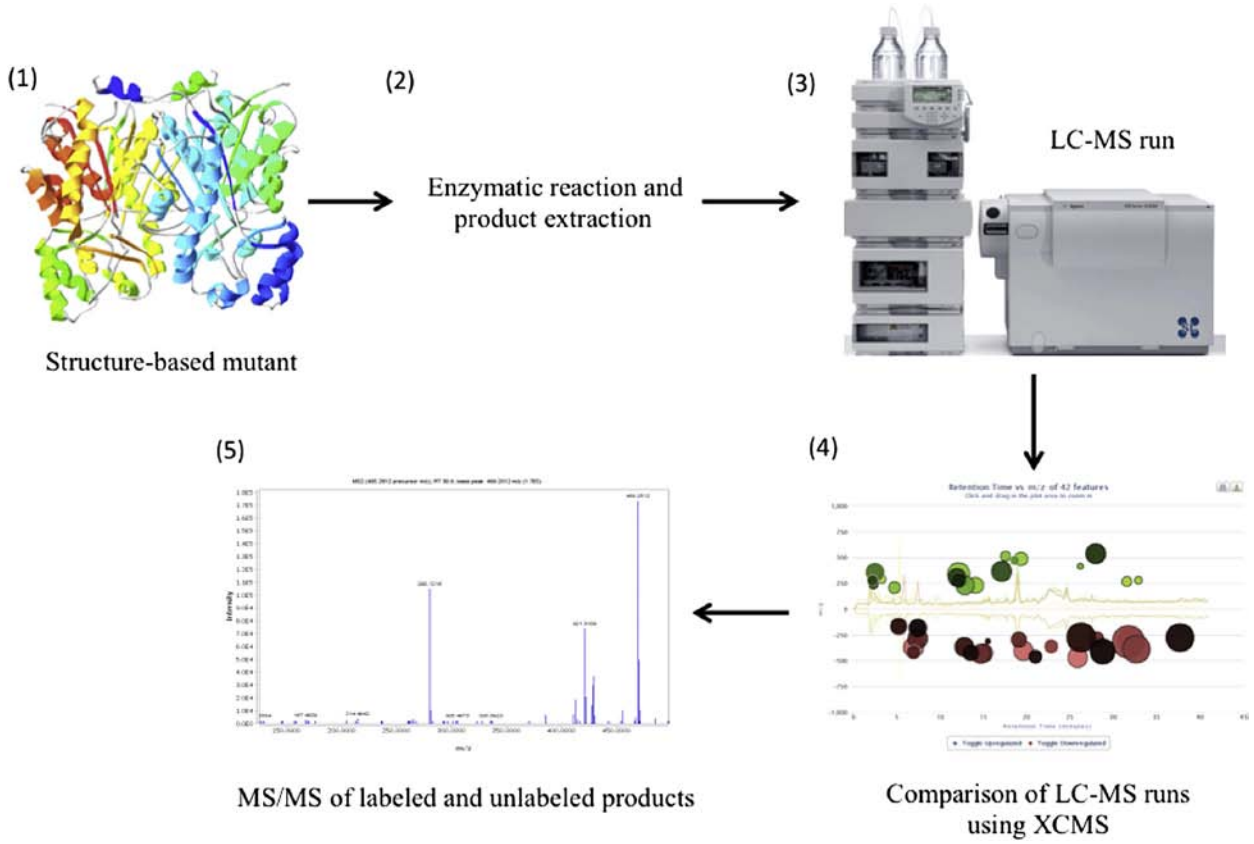

Fig. 6. XCMS based workflow for quick identification of novel PKs formed. (1) Create structure-based mutants. (2) Carry out *in vitro* reaction with and without ^{13}C labeled substrate. (3) Carry out LC-MS analysis. (4) XCMS analysis of online XCMS data. (5) MS/MS analysis of interesting peaks identified via XCMS analysis.

Several other possible combinations of substrates, with a range of different sizes and polarities, could be tested, to afford a comprehensive expansion of the PK space, although testing all of these possible combinations is beyond the scope of this work. Upon feeding non-natural substrates to the different mutants we were able to further diversify the PK space by generating 9 additional non-natural PKs that have not been previously reported. All of the PKs characterized in this study are unique to STS-like enzymes, establishing STS as a candidate enzyme for future protein engineering efforts and as a tool for generation of libraries of novel PKs with potential therapeutic value. Finally, XCMS analysis was utilized for quick identification of PKs that were formed only by the mutants, and the established workflow aided in simple and rapid identification of all 15 novel, non-natural PKs directly from the online HR-LCMS data.

We propose that this quick identification workflow can be utilized for generation of many more novel PKs. In the future, supplementation with nitrogen-containing substrates could help generate novel non-natural alkaloid analogs. Further optimization of the biosynthetic production of these novel PKs can be carried out, as has been previously reported [30–35].

Conflict of interest

None.

Acknowledgments

The authors would like to thank Dr. Dmitri Zagorevski for help with LC-MS analysis. This work was partially supported using funding provided by the RPI Biocatalysis Constellation. The authors acknowledge no conflict of interest.

Appendix A. Supplementary data

Supplementary data related to this article can be found at http://dx.doi.org/10.1016/j.biochi.2015.05.019.

References

[1] C. Stewart Jr., C.R. Vickery, M.D. Burkart, J.P. Noel, Confluence of structural and chemical biology: plant polyketide synthases as biocatalysts for a bio-based future, Curr. Opin. Plant Biol. 16 (2013) 365–372.
[2] I. Abe, Novel applications of plant polyketide synthases, Curr. Opin. Chem. Biol. 16 (2012) 179–185.
[3] B. Agarwal, J.A. Baur, Resveratrol and life extension, Resveratrol Health 1215 (2011) 138–143.
[4] Q. Xu, L.-Y. Si, Resveratrol role in cardiovascular and metabolic health and potential mechanisms of action, Nutr. Res. 32 (2012) 648–658.
[5] N. Jang, J. Cai, G.O. Udeani, K.V. Slowing, C.F. Thomas, C.W. Beecher, H.H. Fong, N.R. Farnsworth, A.D. Kinghorn, R.G. Mehta, R.C. Moon, J.M. Pezzuto, Cancer chemopreventive activity of resveratrol, a natural product derived from grapes. Science 275 (1997) 218–220.
[6] M. Böhm, S. Rosenkranz, U. Laufs, Alcohol and red wine: impact on cardiovascular risk, Nephrol. Dial. Transpl. 19 (2004) 11–16.
[7] G. Chen, W. Shan, Y. Wu, L. Ren, J. Dong, Z. Ji, Synthesis and anti-inflammatory activity of resveratrol analogs, Chem. Pharm. Bull. (Tokyo) 53 (2005) 1587–1590.
[8] M.A. Birrell, K. McCluskie, S. Wong, L.E. Donnelly, P.J. Barnes, M.G. Belvisi, Resveratrol, an extract of red wine, inhibits lipopolysaccharide induced airway neutrophilia and inflammatory mediators through an NF-kappaB-independent mechanism. FASEB 19 (2005) 840–841.
[9] S.L. Wu, C.E. Pan, L. Yu, K.W. Meng, Immunosuppression by combined use of cyclosporine and resveratrol in a rat liver transplantation model. Transpl. Proceed. 37 (2005) 2354–2359.

[10] S.L. Wu, L. Yu, K.W. Meng, Z.H. Ma, C.E. Pan, Resveratrol prolongs allograft survival after liver transplantation in rats. World J. Gastroenterol. 11 (2005) 4745–4749.
[11] D. Vauzour, Dietary polyphenols as modulators of brain functions: biological actions and molecular mechanisms underpinning their beneficial effects, Oxid. Med. Cell. Longev. 2012 (2012), 914273–914273.
[12] P. Maher, R. Dargusch, J.L. Ehren, S. Okada, K. Sharma, D. Schubert, Fisetin lowers methylglyoxal dependent protein glycation and limits the complications of diabetes, Plos One 6 (2011).
[13] N. Funa, Y. Ohnishi, I. Fujii, M. Shibuya, Y. Ebizuka, S. Horinouchi, A new pathway for polyketide synthesis in microorganisms,, Nature 400 (1999) 897–899.
[14] Y. Katsuyama, Y. Ohnishi, Type III polyketide synthases in microorganisms, in: D.A. Hopwood (Ed.), Nat. Prod. Biosynth. Microorg. Plant, Pt A, Elsevier Academic Press Inc, San Diego, 2012, pp. 359–377.
[15] D. Yu, F. Xu, J. Zeng, J. Zhan, Type III polyketide synthases in natural product biosynthesis, Iubmb Life 64 (2012) 285–295.
[16] H. Morita, M. Yamashita, S.-P. Shi, T. Wakimoto, S. Kondo, R. Kato, S. Sugio, T. Kohno, I. Abe, Synthesis of unnatural alkaloid scaffolds by exploiting plant polyketide synthase, Proc. Natl. Acad. Sci. U. S. A. 108 (2011) 13504–13509.
[17] I. Abe, Engineering of plant polyketide biosynthesis, Chem. Pharm. Bull. 56 (2008) 1505–1514.
[18] I. Abe, Engineered biosynthesis of plant polyketides: structure-based and precursor-directed approach, Top. Curr. Chem. 297 (2009) 45–66.
[19] M.B. Austin, M.E. Bowman, J.L. Ferrer, J. Schroder, J.P. Noel, An aldol switch discovered in stilbene synthases mediates cyclization specificity of type III polyketide synthases, Chem. Biol. 11 (2004) 1179–1194.
[20] G. Hrazdina, F. Kreuzaler, K. Hahlbrock, H. Grisebach, Substrate specificity of flavanone synthase from cell suspension cultures of parsley and structure of release products in vitro, Arch. Biochem. Biophys. 175 (1976) 392–399.
[21] N. Bhan, L. Lin, C. Cai, P. Xu, R.J. Linhardt, M.A.G. Koffas, Enzymatic formation of a resorcylic acid by creating a structure-guided single-point mutation in stilbene synthase, Prot. Sci. 24 (2014) 167–173.
[22] J. Stockigt, M.H. Zenk, Chemical synthesis and properties of hydroxycinnamoyl coenzyme A deriatives. Zeitschrift Fur Naturforschung C-a J. Biosci. 30 (1975) 352–358.
[23] R. Tautenhahn, G.J. Patti, D. Rinehart, G. Siuzdak, XCMS online: a web-based platform to process untargeted metabolomic data,, Anal. Chem. 84 (2012) 5035–5039.
[24] N. Guex, M.C. Peitsch, SWISS-MODEL and the Swiss-PdbViewer: an environment for comparative protein modeling, Electrophor. 18 (1997) 2714–2723.
[25] R.A. Laskowski, J.C. Rullmann, M.W. MacArthur, R. Kaptein, J.M. Thornton, AQUA and PROCHECK-NMR: programs for checking the quality of protein structures solved by NMR, J. Biomol. NMR 8 (1998) 477–486.
[26] J. Liang, H. Edelsbrunner, C. Woodward, Anatomy of protein pockets and cavities: measurement of binding site geometry and implications for ligand design, Prot. Sci. 7 (1998) 1884–1897.
[27] H. Morita, H. Noguchi, J. Schroder, I. Abe, Novel polyketides synthesized with a higher plant stilbene synthase, Euro, J. Biochem. 268 (2001) 3759–3766.
[28] I. Abe, T. Watanabe, H. Noguchi, Enzymatic formation of long-chain polyketid pyrones by plant type III polyketide synthases, Phytochem. 65 (2004) 2447–2453.
[29] C.A. Smith, E.J. Want, G. O'Maille, R. Abagyan, G. Siuzdak, XCMS: processing mass spectrometry data for metabolite profiling using nonlinear peak alignment, matching, and identification, Anal. Chem. 78 (2006) 779–787.
[30] C.G. Lim, Z.L. Fowler, T. Hueller, S. Schaffer, M.A. Koffas, High-yield resveratrol production in engineered *Escherichia coli*, Appl. Environ. Microbiol. 77 (2011) 3451–3460.
[31] N. Bhan, P. Xu, O. Khalidi, M.A.G. Koffas, Redirecting carbon flux into malonyl-CoA to improve resveratrol titers: proof of concept for genetic interventions predicted by OptForce computational framework, Chem. Eng. Sci. 105 (2012).
[32] N. Bhan, P. Xu, M.A.G. Koffas, Pathway and protein engineering approaches to produce novel and commodity small molecules, Curr. Opin. Biotech. 24 (2013) 1137–1143.
[33] B.F. Cress, Ö.D. Toparlak, S. Guleria, M. Lebovich, J.T. Stieglitz, J.A. Englaender, J.A. Jones, R.J. Linhardt, M.A.G. Koffas, CRISPathBrick: modular combinatorial assembly of type II-a CRISPR arrays for dCas9-mediated multiplex transcriptional repression in *E. coli*. ACS Synth. Biol. (2015) [Epub ahead of print].
[34] S. Zhao, J.A. Jones, D.M. Lachance, N. Bhan, O. Khalidi, S. Venkataraman, Z. Wang, M.A.G. Koffas, Improvement of catechin production in *Escherichia coli* through combinatorial metabolic engineering, Metab. Eng. 28 (2015) 43–53.
[35] P. Xu, N. Bhan, M.A.G. Koffas, Engineering plant metabolism into microbes: from systems biology to synthetic biology, Curr. Opin. Biotech. 24 (2013) 291–299.